The High Altitude X-Ray Detector Testbed Payload for the 2014 High Altitude Student Platform

Technical Points of Contact
Seth Frick <frick100@umn.edu>
Josiah DeLange <delan231@umn.edu>

Advisor: Demoz Gebre-Egziabher
University of Minnesota – Twin Cities

Abstract

The results of analysis of the data collected from the University of Minnesota High Altitude X-ray Detector Testbed (HAXDT) payload on the 2014 High Altitude Student Platform (HASP) flight are described. The objective of HAXDT is to test the performance of and acquire space heritage for a low-cost, compact X-ray detector system. The detector systems are being developed as part of a program to explore the possibility of using natural, celestial X-ray sources as navigation beacons to enable autonomous, deep-space navigation capability for future spacecraft. The data showed that the detector systems operated successfully in a near-space environment, recording photon events in the energy range of 100 keV to 8 MeV; however, one of the two detectors used showed signs of performance degradation due to aging. Furthermore, lessons learned in the design and testing of the payload are described and documented so that the design of further payload iterations can be improved for future HASP missions.

Introduction

The University of Minnesota's (UMN) High Altitude X-ray Detector Testbed (HAXDT) is a high altitude balloon payload developed to test and validate the performance of compact, low-power, low-cost X-ray and gamma-ray detectors and their associated flight hardware on Louisiana State University's (LSU) High Altitude Student Platform (HASP). The HAXDT payload consists of a flight computer and daughter board; onboard flash storage; attitude and navigation sensors (IMU and GPS); a power regulation and protection circuit; and two small detectors capable of capturing high-energy photon events along with their associated hardware.

The impetus for developing a small detector system is that many envisioned deep space missions, such as long-range sample return or interplanetary reconnaissance, will require space vehicles to have autonomous navigation capabilities. With these capabilities, such vehicles will not have to remain in constant contact with Earth. Such autonomy could relieve reliance upon Earth-based monitoring systems such as NASA's Deep Space Network (DSN). Recent work has shown that celestial X-ray sources such as pulsars can be used as navigation beacons for determining the absolute position of space vehicles [1-13]. Pulsars occur naturally over immense astronomical distances, and thus navigation systems which utilize them in a navigation solution will not have to rely on Earth-based operations.

Pulsars are excellent candidates for navigation beacons because their unique, identifying signals can be used to provide time, range, and range-rate measurements, which are key parameters in obtaining an accurate navigation solution [13]. However, because pulsars occur many parsecs from Earth, the signal-to-noise ratio (SNR) of the received X-ray signals is small [13]. Further, the performance of a small detector receiving such signals is relatively unknown. Such small detectors could easily and affordably be placed on a fleet of autonomous spacecraft. The primary objective of the UMN HASP experiments, namely HAXDT, is to provide a platform which can be used to evaluate, analyze, and gain flight heritage for such detectors. This is crucial to the development of an autonomous, low-cost deep space X-ray navigation system.

In previous years, the HAXDT payload was designed to conform to CubeSat generic structure standards, based on one or more cubes with internal dimensions of 10 cm x 10 cm x 10 cm. A single cube is known as a 1-U, or unit volume, configuration. The 2014 version of HAXDT is a modified 3-U payload as shown in the 3D drawing in Figure 1 below, with the base dimensions increased to 13 cm x 13 cm to accommodate a reinforced structure and allow for easier integration of the payload components. Although this modification was made for the 2014 payload, all of the payload components can still fit readily into a standard 3-U CubeSat structure, and thus the proposed applicability of the HAXDT detector systems to a CubeSat platform is still valid. The payload is ultimately being designed to test the system in space, thus the CubeSat model provides a flexible platform that can be modified for future HASP missions as well as space flight opportunities.

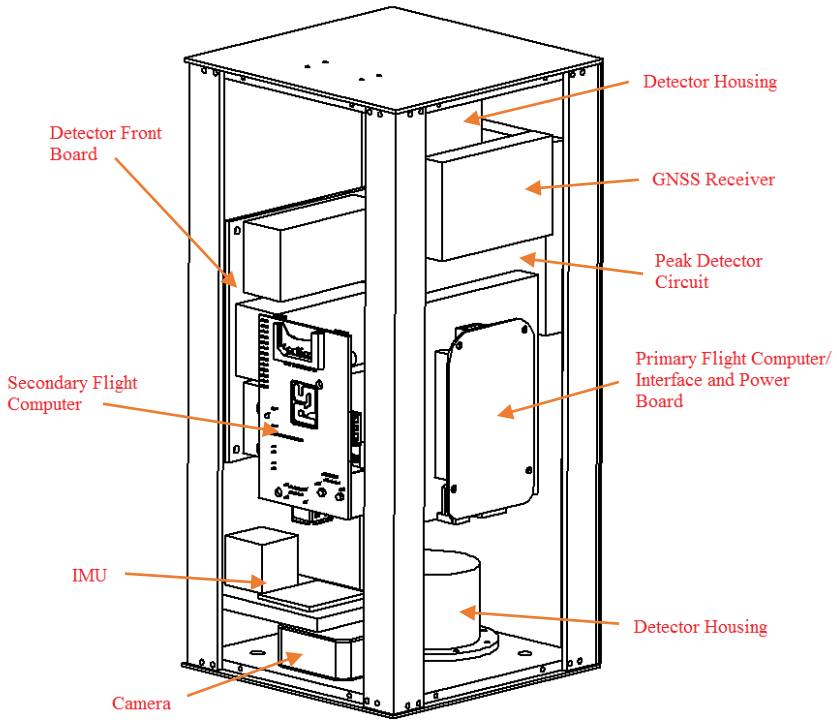

Figure 1. A 3D drawing of the HAXDT structure. The base is 13 cm x 13 cm, while the wall is 30 cm high. Note that the payload is reinforced with structural angles on the edges. All interior hardware is custom mounted as indicated. The detectors sit in the cylindrical mounts as shown attached to the interior of the upper and lower plates. The GNSS antenna sits on top of the payload, but it is not shown here.

The HAXDT hardware consists mainly of commercially available and OEM components, but also includes some custom-developed parts. The primary flight computer is a BeagleBone Black, an open-source development board built around the Texas Instruments AM3358 Sitara SoC. The AM3358 is a 32-bit ARM Cortex-A8 processor and runs a stripped version of Debian GNU/Linux. A custom-designed cape board handles the hardware interfaces to the flight computer. This cape board also serves as a power supply for the payload, including overvoltage protection and current limiting. The flight code was written in C language. Upgrades from the 2013 code include binary data logging to a microSD card, an improved technique for interrupt handling, and a simplified code structure based on state machines and parallel processing.

The primary function of the flight code was to store the energy levels of scintillation events without any significant delay, which required hardware-driven interrupt capabilities. This was accomplished using a kernel-space module that logged the digital values returned by the peak detector circuit each time a photon struck one (or both) of the detectors. When an event occurred the resulting digital values, corresponding to photon energy levels, of both detectors were stored on the microSD card along with the time that the events occurred (precise to the microsecond). The other function of the flight code was to log data from the GNSS receiver and IMU, which was accomplished in the main loop. Note that the kernel module and main loop are separate processes, so a malfunction in one does not necessarily eliminate both modes of data acquisition. The GNSS data is acquired using a NovAtel OEMStar receiver, which is capable of receiving both GPS L1 and GLONASS L1 signals. The OEMStar is suitable for use on a high altitude flight, since it complies with export control restrictions by limiting operation to a maximum velocity of 1,000 knots, rather than limiting the operation to a maximum altitude of 60,000 feet. The IMU is an Analog Devices ADIS16405 and provides angular rates, accelerations, magnetic field, and temperature readings. A precise

navigation and attitude solution may be obtained by fusing the GNSS position with a filtered attitude solution from the IMU.

The detector assemblies are seated in aluminum housings as shown in Figure 2 below. Each assembly consists of an avalanche photodiode (APD) affixed to a plastic organic scintillator with optical grease, which is then wrapped in polytetraflouroethylene (PTFE) tape. Visible light flashes generated by high-energy particle interactions with the scintillator are collected and converted to a charge pulse by the APD. The pulses are shaped and amplified by a nuclear pulse-shaping circuit (detector board) designed by Lockheed Martin's Advanced Technology Center in Palo Alto, CA. The detector board also provides the high-voltage supply required to bias the APD (approximately 400V). Pulse height analysis is performed in real time by custom circuitry consisting of high-speed op amps and an analog-to-digital converter with a temperature-stable external voltage reference. Photon strikes are time-tagged by the flight computer using the discriminator output of the detector board to drive an interrupt, and photon energy levels are recorded as voltage measurements from the pulse height analysis circuitry. The scintillator and APD were selected to produce a detector with a peak sensitivity in the range of 100 keV–5 MeV, corresponding to gamma-rays which can be easily observed in the Earth's atmosphere. As mentioned earlier, the signal-to-noise ratio of X-rays in the Earth's atmosphere is very low, making the detection of actual X-rays exceptionally difficult, even at high altitudes. The detector is also somewhat sensitive to higher energy particles in the range of 5–20 MeV, such as fast neutrons.

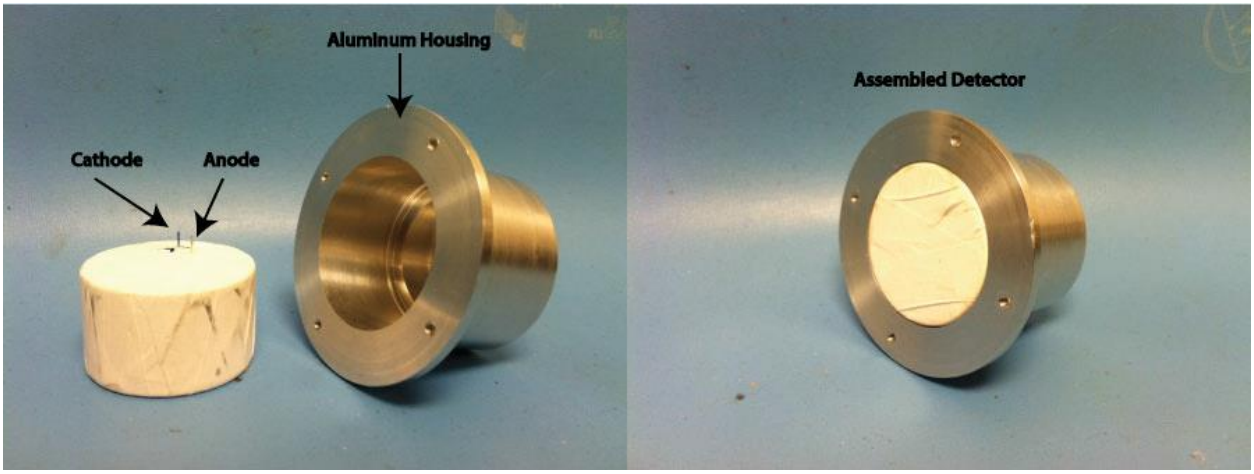

Figure 2. The HAXDT detector is comprised of an APD attached to a plastic scintillator and then wrapped in PTFE tape. Shown are the cathode and anode of the APD protruding from the PTFE tape (left). The wrapped assembly is then seated in the aluminum housing to complete the assembled detector (right).

Payload Performance

The 2014 HAXDT payload met all performance expectations in ground testing leading up to the HASP flight. The GNSS receiver and IMU were able to provide stable and reliable navigation and attitude data for the payload, and the detectors successfully recorded scintillation events at energy levels ranging from 100 keV–8 MeV, as measured by the pulse height analysis circuitry.

In addition to meeting the performance thresholds established by the UMN HASP team, the HAXDT payload stayed within the specified mechanical and electrical limits required for proper integration with the HASP flight equipment. The measured weight of the payload including the payload plate was 2.91 kg, within the 3 kg limit. Further, the measured current draw of the payload from the 30V supply was 180 mA, well below the 500 mA limit. The current draw remained relatively stable over the full range of temperature

and pressure conditions tested, from −50 °C to 50 °C, and from sea-level pressure down to about 10 millibar. However, the flight computer malfunctioned during thermal testing. The telemetry packets contained invalid data, which suggested either the processor had experienced some sort of issue or the code had malfunctioned (in particular, the kernel buffer had overflowed due to inefficient memory management). The computer still logged photon events however, and although the telemetry failed, the primary experiment remained intact. The code was examined and fixed shortly thereafter.

Despite the software issues experienced during integration testing, the HAXDT payload performed very well throughout the actual HASP flight. During the flight, the payload successfully recorded photon events and IMU data, and downlinked status information and telemetry packets. However, the GNSS receiver performed very poorly, managing to record only about a dozen positions throughout the flight. This was originally thought to be due to incorrect interfacing with the receiver in the flight software, but this theory was disproved in successful ground tests after the flight. To further evaluate the capabilities of the OEMStar in a high-altitude environment, the receiver was re-flown locally on a sounding balloon with another student group at UMN. The OEMStar was flown in a similar configuration to the HASP flight. However, the small, inexpensive patch antenna used on the HASP flight was replaced with a more robust NovAtel-certified antenna. With this change, the receiver performed perfectly throughout the entire flight.

While the original design for the 2014 HAXDT payload also included a secondary experiment which would use a downward-looking camera to aid in attitude determination, this experiment was excluded from the project at a late stage due to a lack of available time for development. This experiment would have fulfilled in part the work of Haley Rorvick for a UMN-funded Undergraduate Research Opportunities Program (UROP) project on the application of a camera for attitude determination of an airborne payload.

Problems Encountered and Lessons Learned

The HASP project came together with a few, minimal setbacks, and the development of the payload was largely considered a success. However, like any other engineering project, there were several challenges and minor issue that arose during the design, build, and testing of the 2014 HAXDT payload. Dealing with these challenges produced many valuable lessons which will be applied to future iterations of the project in hopes of mitigating such issues.

1. Greater care will be taken in machining the payload's structure. While the top/bottom plates and the side panels were machined initially according to the design, the holes into which the structural supports were to be bolted were not lined up properly, which essentially rendered the entire structure unable to be assembled. This added an unnecessary setback in the schedule of the build phase of the project, since the design and fabrication of the structural components was done exclusively by one or two team members who had subsequently been completely unavailable due to other jobs during the summer.
2. Only two team members were available during this time and the initial schedule had assumed the structure would be completed before the summer, when the software would be designed and tested. Since the structure needed to be redone, the camera experiment was excluded entirely from the mission due to a lack of time available to develop/test its operation. In future project cycles there will be a more dedicated effort to finish the structure much earlier in the project cycle, so that no work needs to be redone.
3. More time was spent figuring out how to make the code work than was spent testing it for failure modes. Both the analog-to-digital converter in the peak detector circuit and the IMU use a serial peripheral interface (SPI) bus. Often with open-source development boards there is code made available by the open-source community to aid development. A few SPI libraries were available for the BeagleBone Black; however, upon testing they were found to be non-functional. Drivers

for the IMU and peak detector were hard-coded from a standpoint of Linux input/output methods. Similarly, the flight computer's GPIO pins are multiplexed, so time was also spent writing the correct data structure to set the pins' modes at boot time. Interrupt handling was to be done by design using a hardware-driven method to record periods of high photon flux. However, the version of Linux used relied only on software interrupts, and the kernel module to handle the hardware interrupts also required a significant amount of research in order to ensure its robustness. Documentation for Linux is often too sparse for the level of technical involvement that was required for the HAXDT project. These shortcomings coupled with an unfinished payload cost the team time that could have been used to thoroughly test the primary flight code. In future project cycles, this type of work should be started much earlier, and thoroughly documented.

4. The current payload design does not allow for the flight computer to be accessed remotely through a wireless connection such as WiFi or Bluetooth. During thermal/vacuum testing, a mistake in the main loop caused the telemetry packets to fail to send and the team had no idea what had happened initially. Although not crucial to success, this could be easily mitigated by a USB WiFi transceiver. This would have been a useful tool to have during the thermal/vacuum test because the malfunction of the software could have been easily fixed and the flight computer rebooted.
5. Code was still being tested at integration. The GNSS receiver's output format was reconfigured from ASCII to binary which involved a CRC calculation, requiring testing and code rewrites. This was done at the very "last minute" prior to flight certification, adding some uncertainty to any potential failures of the code due to a lack of available time to test specific failure modes.
6. In an effort to provide the flight computer with accurate timing capabilities that would not drift significantly over time or with large temperature variations, the flight software was designed to periodically set the flight computer's system clock using the time from the GNSS receiver. Timestamps for all logged data would then be generated in microsecond precision from the system clock, with accuracy assured in the assumption that the system clock would be updated with GPS time before instabilities in the BeagleBone Black's onboard oscillator could propagate into large errors. The system clock was set by parsing the incoming GPS data to obtain the GPS week number and time of week. However, because the GNSS receiver failed during the flight, the system clock could not be updated frequently, and as a result the timestamps generated on logged data were inaccurate. Luckily, the data of most interest (the photon energy spectra) did not rely on having accurate timestamps. In the future, we will not rely on having valid GPS data in order to keep accurate time. Instead, we may derive a clock from the pulse-per-second (PPS) output of the GNSS receiver (which is more accurate with a GPS lock, but is far more stable than the BeagleBone Black oscillator even without a lock), or instead use a separate stable timing source such as a chip-scale atomic clock (CSAC). For synchronization purposes, the CSAC could be slaved off of the GNSS receiver PPS output.

Results Summary

I. <u>Detector Calibration</u>

The amplified output of the detector board is simply a voltage pulse, which is sampled by a 10-bit analog-to-digital converter in the pulse height analysis circuitry. The height of the voltage pulse corresponds directly to the energy of the detected particle, but the exact relationship between voltage (i.e. digital values from 0 to 1023) and particle energy is not known a priori. While this relationship can be estimated based on the specifications of the detector systems such as the scintillator light yield, APD quantum efficiency, and shaping amplifier gain, obtaining an accurate estimate in this manner is extremely difficult due to uncertainties in the specifications as well as unmodeled effects. A much better result is found empirically, by testing the detector systems with a known radioactive source in a controlled environment.

The source used for calibration of the HAXDT detector systems was an incandescent gas lantern mantle containing Thorium-232. To properly characterize this source, a test was performed using a previously calibrated off-the-shelf detector system available in the UMN physics department. This detector system consists of a thallium-doped sodium iodide, or NaI(Tl), scintillation crystal; a photomultiplier tube; and a multi-channel analyzer. From this test, we obtained an energy spectrum for the lantern mantle which was considered a truth solution, shown in Figure 3 below. The same test with the lantern mantle was then performed with the HAXDT detector systems, generating an energy spectrum which is also shown in Figure 3. After this test, a linear least-squares regression was done with the main peaks of the truth spectrum and the HAXDT spectrum to obtain the relationship between the HAXDT "channel number" (digital values from 0 to 1023) and the incident particle energy in kiloelectronvolts.

Although the calibration testing was actually performed after the 2014 HASP flight, the calibration data is presented here to allow for better interpretation of the flight data that follows.

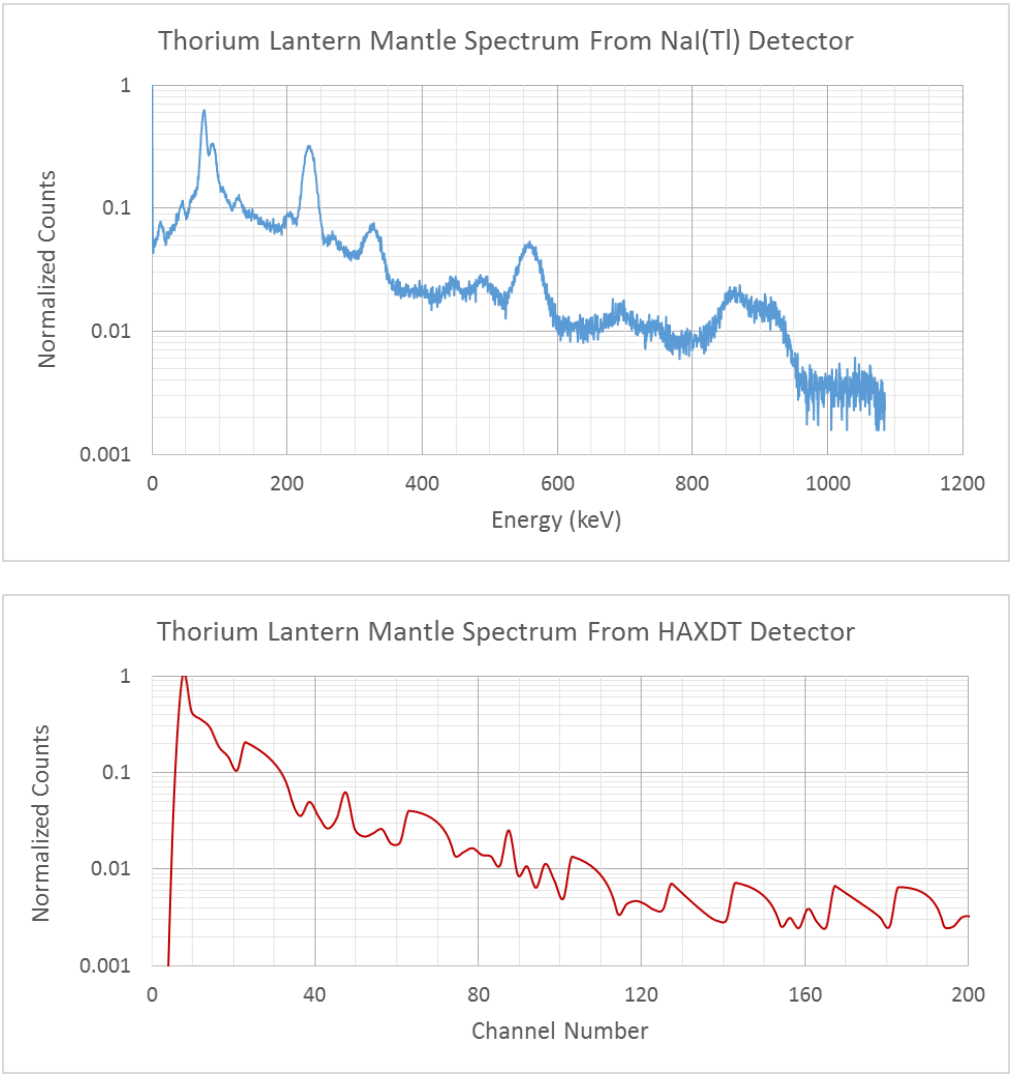

Figure 3. The energy spectra from calibration testing with the thorium lantern mantle are shown, as measured by the commercial NaI(Tl) detector (top), and a HAXDT detector (bottom).

II. Detector Flight Data

As mentioned previously, the HAXDT detector systems performed well during the 2014 HASP flight, with both detectors collecting photon energy measurements throughout the entirety of the flight. The average photon energy spectra measured by each of the detectors over the full duration of the HASP flight are shown in Figure 4 below. The spectra shown are normalized relative to the energy bin with the highest number of counts on each detector, such that the highest peak will have a normalized value of 1.

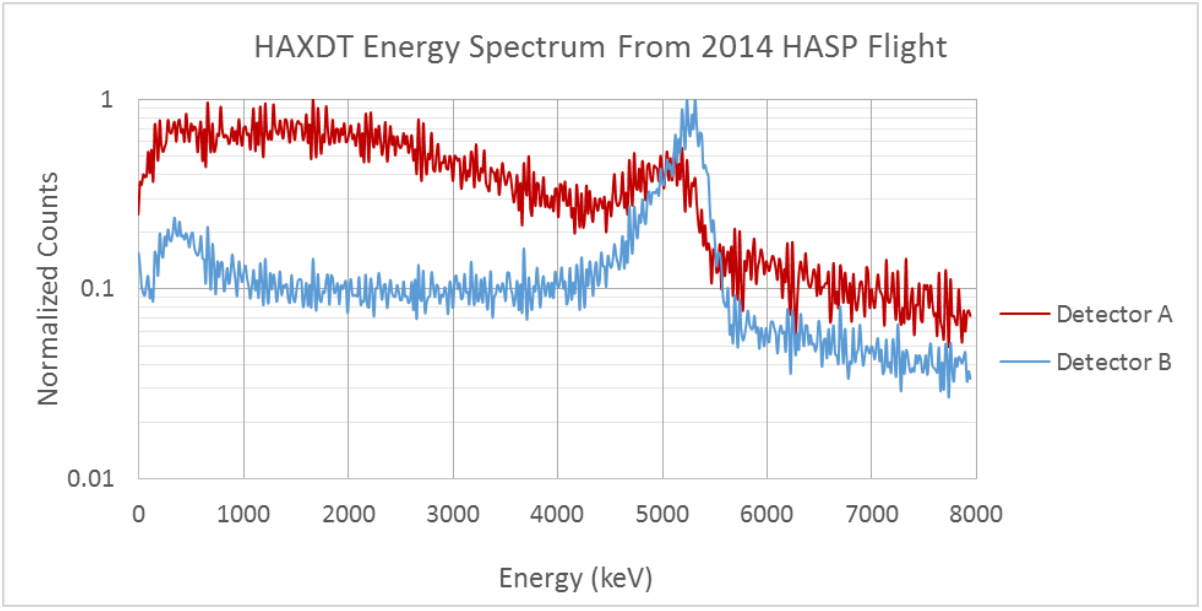

Figure 4. The energy spectra from the 2014 HASP flight are shown, as measured by the two HAXDT detectors.

The detectors measured two significant energy peaks: a small peak at around 400 keV, and a larger peak at around 5.3 MeV. Both detectors are in agreement; however, it can clearly be seen in the figure that Detector A has higher noise and much less pronounced peaks. Further, Detector A measured photon arrivals at an average rate of 3.6 events per second, while Detector B registered an average rate of 5.8 events per second. The reason for Detector A's poorer energy resolution (broadened peaks) and lower overall sensitivity (decreased count rates) compared to Detector B is believed to be due to dead-layer growth and degradation of the scintillator material. Detector A was assembled using a scintillator that is several years old and previously flew on the 2012 HASP flight, while Detector B used a scintillator that was brand new for the 2014 payload. Crystal scintillators are known to be prone to dead-layer growth which can impede their performance [14], and it is understood that plastic scintillators experience similar effects, especially with significant accumulated radiation exposure.

III. Temperature Flight Data

The ambient internal temperature of the HAXDT payload during the 2014 HASP flight, as measured by the IMU, is shown in Figure 5 below. As expected, the temperature decreased rapidly during the ascent, reaching a minimum of -45 degrees Celsius, and then slowly increased during the float phase of the flight, rising to about -5 degrees Celsius. The small oscillations in the temperature during the float phase are due to the slow rotation of the HASP gondola, causing the HAXDT payload to experience periodic intervals of direct sunlight. This slow rotation can be seen in the IMU data as well, particularly the magnetic field measurements. Despite the low ambient temperatures inside the HAXDT payload for the majority of the flight, all payload hardware

continued to function properly, with the exception of the GNSS receiver which did not maintain a position lock due to the low-grade antenna used (although the receiver still remained powered and continued to output data).

It should be noted that the time axis used in the figure is based on the timestamps of the logged data, which were inaccurate due to the GNSS receiver failure, as mentioned in the Problems Encountered and Lessons Learned section. Therefore, the time shown on this axis is not an accurate measure of the time elapsed since the payload powered up prior to flight. According to these timestamps, the HAXDT was powered for a total of 360 minutes; the HASP data records indicate, however, that the payload was powered for 500 minutes. This discrepancy is significant, but since no time-sensitive data analysis was required to evaluate the performance of the payload, no actions were taken to attempt to correct the timestamps. This same time axis is used for all of the data collected from the IMU, which is presented in the following subsection.

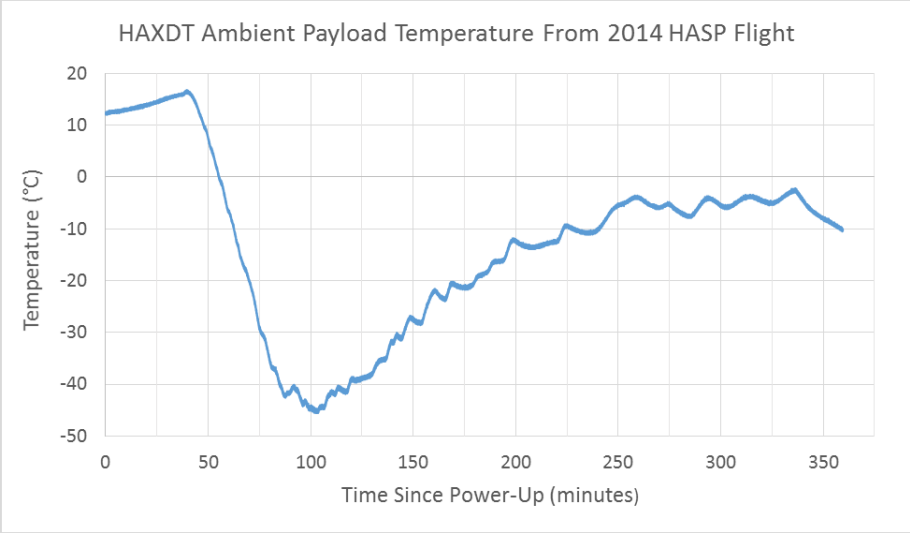

Figure 5. The internal HAXDT payload temperature from the 2014 HASP flight is shown.

IV. IMU Flight Data

The data from the IMU, including three-axis accelerations, angular rates, and magnetic field measurements, are shown in Figures 6–8. The IMU was mounted in the payload in an orientation such that the x-axis of the IMU was aligned with the downward body axis of the payload. The y- and z-axes then defined the horizontal plane of the payload body frame.

The original motivation for collecting these measurements from the IMU was to aid in the development of a high-precision post-processed position and attitude solution for the HAXDT payload throughout the flight. This would be done using traditional sensor fusion techniques such as Kalman filtering to incorporate measurements from the accelerometers, gyroscopes, magnetometers, and GNSS receiver in attaining the navigation and attitude solution. This task was not undertaken in the post-flight data processing for the 2014 HAXDT payload, for a few reasons: (1) the lack of a continuous GNSS position solution inhibits the correction of integration errors which grow without bound over time; (2) the lack of accurate timestamp information for the IMU data complicates the process of generating an accurate solution, and thus a suitable model for the clock errors would first need to be developed; and (3) the precision position and attitude solution is not needed for interpreting the most valuable data from the 2014 flight, namely the detector energy spectra. The capability of generating this precise navigation solution from the IMU and GPS measurements was demonstrated previously with data collected from the 2012 HASP flight.

In spite of the fact that the inertial data was not processed into a complete position and attitude solution, there are still some points to be made about the individual measurements. On the acceleration plot, there is noticeable activity as the HASP gondola is hoisted by the mobile launch vehicle, followed by a large spike when the gondola is released, at approximately 35 minutes on the indicated time axis. During the ascent there are some small accelerations, but the float phase is very stable. Notice also that the x-axis is biased by the Earth's gravitational acceleration, as expected. From the angular rates in Figure 7, we see the same activity as in the acceleration data. However, in this case there is also a rotation about the vertical axis that persists throughout the ascent and slows as the gondola reaches the float phase. The same rotation about the vertical axis can be seen in the y- and z-axis magnetic field measurements in Figure 8. In fact, from this plot the rotation can be tracked even after the rate has slowed enough that it cannot be discerned from the angular rate measurements, well into the float phase. Interestingly, the period of rotation seen in this plot coincides with the fluctuations in temperature seen at float altitude, indicating that the rotation caused the HAXDT payload to come into and out of direct sunlight. It should be noted that the magnetic field measurements shown do not take into account any hard iron or soft iron calibrations. Therefore, the measurements of Earth's magnetic field are biased by effects of the payload structure, HAXDT electrical components, and other electrical components located on the HASP frame.

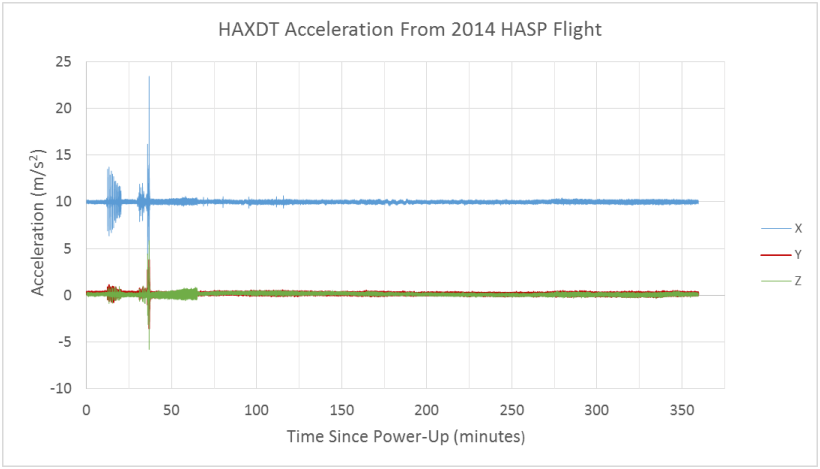

Figure 6. Three-axis acceleration measurements from the 2014 HASP flight, as measured by the HAXDT IMU, are shown.

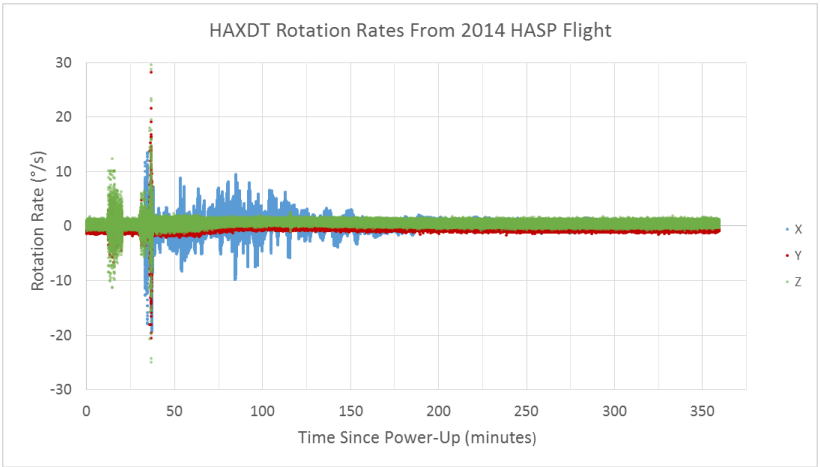

Figure 7. Three-axis angular rate measurements from the 2014 HASP flight, as measured by the HAXDT IMU, are shown.

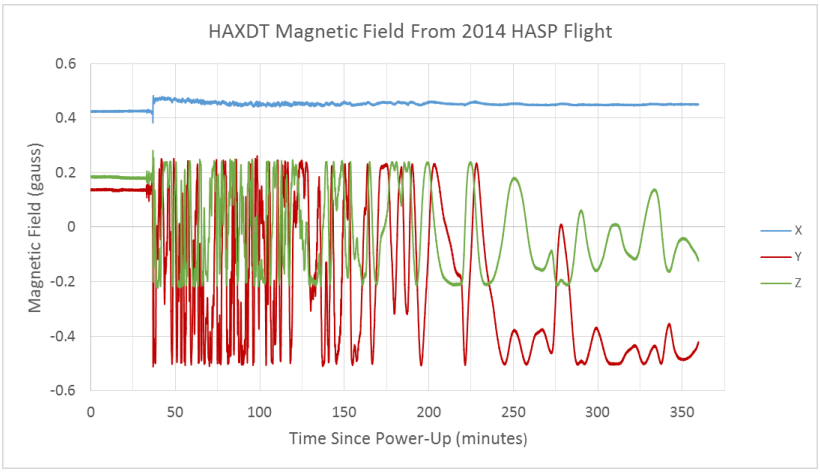

Figure 8. Three-axis magnetic field measurements from the 2014 HASP flight, as measured by the HAXDT IMU, are shown.

V. GPS Flight Data

As discussed earlier, the HAXDT GNSS receiver (NovAtel OEMStar) did not perform well during the 2014 HASP flight. The source of the failure was later determined to be the use of a low-grade antenna, and the proper operation of the OEMStar with a more suitable antenna was confirmed through a second "backup" flight. Although the OEMStar did not provide a continuous position solution for the entire HASP flight, the data points that it did provide (although few in number) were in fact accurate. This is seen in Figure 9, which shows the continuous altitude profile of the flight as measured by the HASP GPS (blue line), and the handful of position measurements from the HAXDT GNSS receiver (red crosses).

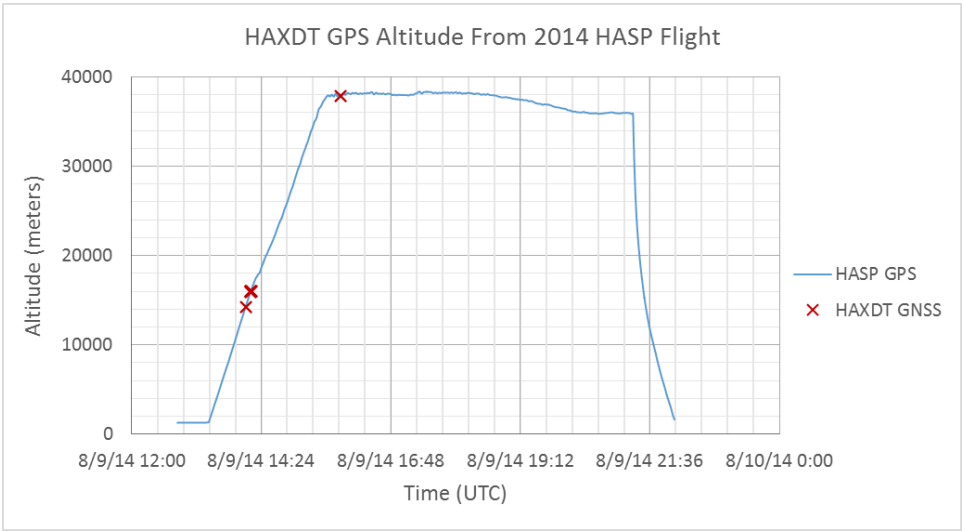

Figure 9. The altitude from the 2014 HASP flight, as measured by the HASP GPS (blue line), is shown. Also shown are the sparse position measurements from the HAXDT GNSS receiver (red crosses).

The second flight of the OEMStar was on November 2, 2014. Members of the HAXDT team collaborated with the UMN ballooning team to launch a 1600 gram latex sounding balloon with several scientific payloads and tracking equipment. The balloon was launched from the small town of Pemberton, MN and flew about 60 kilometers northeast to Moland, MN. Among the payloads was a small box containing the OEMStar with a NovAtel-certified antenna and associated hardware for logging data. The OEMStar performed perfectly in this flight, with no outages, and the altitude

data is shown in Figure 10. The balloon systems used for this flight did not have the ability to float the payloads at a constant altitude, and thus the altitude profile looks quite different from that of the HASP flight. Further, Figure 11 shows the full flight in an extruded 3-dimensional view as well as the ground track, layered over a satellite view in Google Earth.

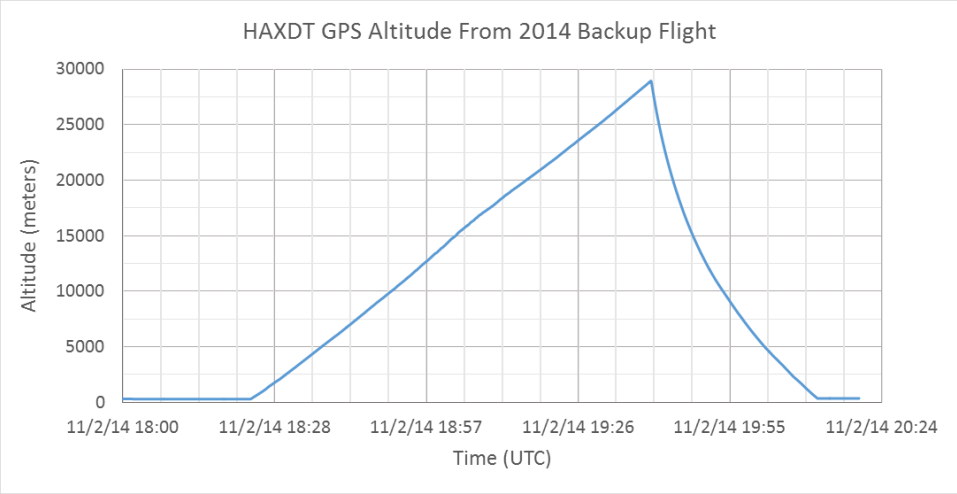

Figure 10. Altitude data measured by the OEMStar receiver on the 2014 backup flight is shown.

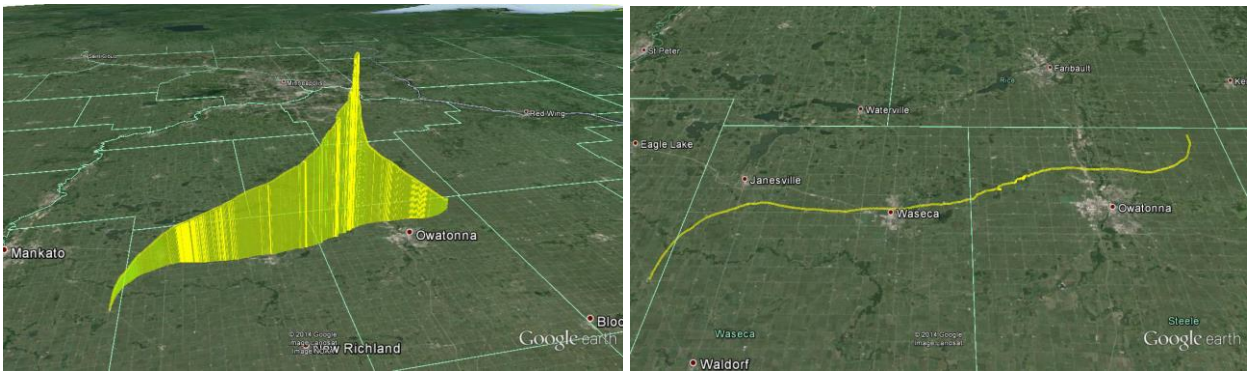

Figure 11. The complete flight path (left) and ground track (right) from the 2014 backup flight, as measured by the OEMStar, are shown in Google Earth.

Conclusions and Future Work

The primary goal of the 2014 HAXDT payload was to reproduce the success of previous HAXDT iterations in detecting and measuring the energy of photon events and collecting navigation and attitude data, with the addition of a second detector and refinement of the photon energy measurements. Although the GNSS receiver failed during the HASP flight, all other payload hardware functioned as intended, and the capabilities of the GNSS receiver were later validated on a second flight. Therefore, the 2014 payload can be declared a success.

The UMN team has several plans for further development and expansion of the HAXDT payload. First and foremost, the payload will be used in the coming years to thoroughly evaluate subsystems and systems for a demonstration CubeSat proposed by ASTER Labs, Inc. under a NASA Small Business Innovations Research (SBIR) grant. ASTER Labs' design includes a detector system similar to the one that has been developed for HAXDT, and seeks to demonstrate the relative navigation of two CubeSats using time

difference of arrival (TDOA) measurements of high-energy photons from gamma-ray burst events (GRBs) from outside the solar system. This will motivate the future direction of the HAXDT detector systems and associated hardware. In addition, the UMN team will be seeking to transition to a large HASP payload, to allow for extensive supporting hardware for the HAXDT experiment beyond the standard CubeSat structure, as well as accommodate secondary experiments and tests. The secondary experiments will be developed as the UMN team expands to incorporate student projects from upper division undergraduate courses in the aerospace engineering and physics departments.

Student Involvement

Below is a table displaying all students involved in the 2014 HASP mission and their demographic information.

Name	Gender	Ethnicity	Race	Student Status	Disability
Seth Frick	M	Non-hispanic	Caucasian	Graduate	No
John Jackson	M	Non-hispanic	Caucasian	Undergraduate	No
Haley Rorvick	F	Non-hispanic	Caucasian	Undergraduate	No
Josiah DeLange	M	Non-hispanic	Caucasian	Undergraduate	No
Alec Forsman	M	Non-hispanic	Caucasian	Undergraduate	No
Seth Merrifield	M	Non-hispanic	Caucasian	Undergraduate	No
Andrew Mahon	M	Non-hispanic	Caucasian	Undergraduate	No

Papers and Presentations

Mr. Frick presented a poster detailing the development of the HAXDT payload and experimental results at the Great Midwestern Regional Space Grant Meeting in Des Moines, Iowa on September 20, 2014.

Acknowledgements

The authors thank Lockheed Martin Space Systems Company's Advanced Technology Center (ATC) for providing the front-end detector board and scintillator material. They especially thank Dr. David Chenette, Mr. Abraham Kou, and Dr. Munther Hindi of ATC for providing valuable time, advice, and laboratory support during the development of the detector system. The authors thank Dr. Keith Gendreau of NASA/GSFC Astrophysics Science Division for his support in detector design. We thank Dr. Suneel Sheikh of ASTER Labs, Inc. for his insight and expertise. The authors would also like to thank Amptek, Inc. and Saint-Gobain Crystal for donating components crucial to the design of the HAXDT detector system. We thank the Louisiana Space Consortium and NASA's Balloon Program Office for supporting annual HASP flights. We also thank Dr. James Flaten, Dr. William Garrard, Kale Hedstrom, and Kurt Wick from the University of Minnesota for their technical advice and assistance. Finally, the authors acknowledge the NASA/Minnesota Space Grant Consortium for providing the funding for this work. While the authors gratefully acknowledge the support from the aforementioned individuals, the views and conclusions

contained in this report are those of the authors alone and should not be interpreted as necessarily representing the official policies, either expressed or implied, of any organization.

References

[1] Hanson, J. E., "Principles Of X-Ray Navigation," Stanford University, 1996, <http://search.proquest.com/docview/304316770/138003114322F6D6003/10?accountid=14586> (17 Jul 2012). il.proquest.com/en-US/products/dissertations/

[2] Sheikh, S. I., "The Use of Variable Celestial X-Ray Sources for Spacecraft Navigation," University of Maryland, 2005, <http://drum.lib.umd.edu/bitstream/1903/2856/1/umi-umd-2856.pdf> (17 Jul 2012). hdl.handle.net/1903/2856

[3] Woodfork, D. W. "The Use of X-ray Pulsars for Aiding GPS Satellite Orbit Determination," Air Force Institute of Technology, <http://www.dtic.mil/cgi-bin/GetTRDoc?AD=ADA437513> (17 Jul 2012). www.dtic.mil/dtic/

[4] Sheikh, S. I., Pines, D. J., Wood, K. S., Ray, P. S., Lovellette, M. N. and Wolff, M. T., "Spacecraft Navigation Using X-Ray Pulsars," Journal of Guidance, Control, and Dynamics 29(1), 49-63 (2006).

[5] Sheikh, S. I. and Pines, D. J., "Recursive Estimation of Spacecraft Position and Velocity Using X-ray Pulsar Time of Arrival Measurements," Navigation: Journal of the Institute of Navigation 53(3), 149-166 (2006).

[6] Sheikh, S. I., Golshan, A. R. and Pines, D. J., "Absolute and Relative Position Determination Using Variable Celestial X-Ray Sources," Proc. AAS 30th Annual Guidance and Control Conference, AAS 07-103, 1-20 (2007).

[7] Sheikh, S. I., Ray, P. S., Weiner, K., Wolff, M. T. and Wood, K. S., "Relative Navigation of Spacecraft Utilizing Bright, Aperiodic Celestial Sources," Proc. ION 63rd Annual Meeting, 444-453 (2007).

[8] Golshan, A. R., and Sheikh, S. I., "On Pulse Phase Estimation and Tracking of Variable Celestial X-Ray Sources," Proc. ION 63rd Annual Meeting, 413-422 (2007).

[9] Graven, P., Collins, J., Sheikh, S. I. and Hanson, J. E., "X-NAV Beyond the Moon," Proc. ION 63rd Annual Meeting, 423-431 (2007).

[10] Ray, P. S., Sheikh, S. I., Graven, P. H., Wolff, M. T., Wood, K. S. and Gendreau, K. C., "Deep Space Navigation Using Celestial X-ray Sources," Proc. ION 2008 National Technical Meeting, 101-109 (2008).

[11] Emadzadeh, A. A., "Relative Navigation Between Two Spacecraft Using X-ray Pulsars," University of California, Los Angeles 2009, <http://proquest.umi.com/pqdlink?did=2055189291&Fmt=7&clientId=2256&RQT=309&VName=PQD> (17 Jul 2012). gradworks.umi.com/34/10/3410447.html

[12] Sheikh, S. I., Hanson, J. E., Graven, P. H. and Pines, D. J., "Spacecraft Navigation and Timing Using X-ray Pulsars," Navigation: Journal of the Institute of Navigation, 58(2), 165-186 (2011).

[13] Doyle, P. T., Gebre-Egziabher, D., and Sheikh, S. I., "The Use of Small X-Ray Detectors for Deep Space Relative Navigation," Proc. of SPIE, 8519, 85190K-1 – 85190K-12 (2012).

[14] Goodman, N. B. "The Growth of Deactivated Layers on CsI(Na) Scintillating Crystals," Laboratory for Solar Physics and Astrophysics, NASA Goddard Space Flight Center, 1975, <http://ntrs.nasa.gov/archive/nasa/casi.ntrs.nasa.gov/19750022825.pdf> (27 Nov 2014).